Cement and Concrete Research 40 (2010) 1555–1570

Contents lists available at ScienceDirect

Cement and Concrete Research

journal homepage: http://ees.elsevier.com/CEMCON/default.asp

Influence of self heating and Li_2SO_4 addition on the microstructural development of calcium aluminate cement

Christophe Gosselin *, Emmanuel Gallucci, Karen Scrivener

Ecole Polytechnique Fédérale de Lausanne (EPFL), Laboratoire des Matériaux de Construction (LMC), Switzerland

ARTICLE INFO

Article history:
Received 2 February 2010
Accepted 29 June 2010

Keywords:
Calcium aluminate cement (D)
Microstructure (B)
Lithium sulphate (D)
Self heating (A)

ABSTRACT

Hydrated Calcium Aluminate Cement (CAC) is known to have a complex microstructure involving different phase assemblages strongly dependant on the temperature. This work presents an experimental approach to study the microstructure of CAC pastes from the first minute of hydration with controlled time–temperature histories up to several months of curing. The self heating usually occurring in the CAC concrete is considered and its influence on the growth and assemblage of the hydration products and subsequent space filling is shown. Quantification of the degree of CA hydration by BSE image analysis is used to understand the evolution of phases throughout the hydration process. Lithium sulphate is commonly used to control the setting time of CAC based materials. It is shown that this promotes the formation of more stable hydrates, but slightly reduces the extent of CA hydration.

1. Introduction

The performance of CAC based materials is related to their properties of rapid hardening and high resistance to chemically aggressive environments. Compared to systems based on OPC, CAC remains a relatively little studied material in the field of cement and concrete science. However several studies have been carried out during the past few decades to understand the mechanisms of CAC hydration [1]. The hydration and microstructural development of CAC are controlled by time, temperature and W/C ratio. In particular, at low temperatures the formation of the stable hydrates C_3AH_6 and AH_3 is preceded by the formation of metastable phases CAH_{10} and C_2AH_8 and amorphous aluminium hydroxide, which convert into the thermodynamically stable phases over time. Because the solubility of C_3AH_6 is the lowest, its precipitation from solution involves the dissolution of the metastable hydrates. These thermodynamic reactions cannot be avoided and have two consequences. First, because the stable hydrates are denser than the metastable ones, the space filled by hydrates decreases as conversion occurs, i.e. as porosity increases. Secondly, because the stable hydrates contain less water than the metastable ones, free water is released by conversion which allows further hydration of unreacted cement, which fills porosity. For this reason it is possible to obtain good mechanical properties from converted CACs if the original water to cement ratio is kept low (below about 0.4).

The main reactive anhydrous compound in calcium aluminate cements is monocalcium aluminate $CaO \cdot Al_2O_3$ (CA). In the literature, only the hydration of CA is considered and the reactivity of secondary reactants, such as gehlenite $CaO \cdot SiO_2 \cdot Al_2O_3$ (C_2AS), is seldom mentioned. Pure C_2AS has a very low reactivity at ambient temperature [2] but this phase reactivity can be enhanced by the presence of impurities such as C_5A_3 incorporated during the sintering of white CAC as suggested by Scrivener et al. [3]. The formation of Stratlingite from the reaction of silica with the metastable hydrates of CAC in blended systems using slag, fly ash or silica fume has been reported [4–7]. However small amounts of C_2ASH_8 are also found in plain CACs, where the silica must come from β-C_2S or C_2AS. Midgley et al. [8] assumed that the presence of C_2ASH_8, observed in *Fondu cement* hydrated for 90 days at 20 °C, could be explained by the reaction between C–S–H from β–C_2S hydration and CAH_{10}. The present work gives new results on the precipitation of C_2ASH_8 in pure CAC systems containing C_2AS.

Studies on CAC hydration are generally carried out under isothermal conditions and the influence of self heating on the phase assemblage has never been studied in detail. In this work CAC paste is hydrated with controlled time–temperature histories simulating the self heating usually occurring in CAC concrete sections. A systematic experimental approach allowed the microstructure to be studied from an early age with two different thermal histories: a temperature rise up to 50 °C (as recorded in a 12 cm thick slab made of CAC concrete) leading to the precipitation of C_2AH_8 and AH_3, and a temperature rise up to 70 °C (by direct immersion at this temperature and by a 10 °C h^{-1} temperature ramp from 20 to 70 °C) to study the formation of the stable assemblage $C_3AH_6 + AH_3$.

* Corresponding author. Ecole Polytechnique Fédérale de Lausanne, STI-MXG 241-Station 12, CH-1015 Lausanne, Switzerland. Tel.: +41 21 693 4382; fax: +41 21 693 5800.
E-mail address: christophe.gosselin@epfl.ch (C. Gosselin).

0008-8846/$ – see front matter © 2010 Elsevier Ltd. All rights reserved.
doi:10.1016/j.cemconres.2010.06.012

Eqs. (1)–(5) recall the possible reactions during the hydration of CA and the conversion of hydration products.

$$CA + 10H \rightarrow CAH10 \quad (1)$$

$$2CA + 11H \rightarrow C_2AH_8 + AH_3 \quad (2)$$

$$3CA + 12H \rightarrow C_3AH_6 + 2AH_3 \quad (3)$$

$$2CAH_{10} \rightarrow C_2AH_8 + AH_3 + 9H \quad (4)$$

$$3C_2AH_8 \rightarrow 2C_3AH_6 + AH_3 + 9H \quad (5)$$

Lithium salts are well known to accelerate the hydration of CACs. Various hypotheses have been advanced relating the precipitation of lithium aluminate hydrate [9–13] acting as seeds for more stable hydration products. In particular the theory of Rodger et al. [11] suggested that aluminate released by hydrolysis of the cement is immediately precipitated as hydrated lithium aluminate. Therefore aluminate ions are detected in solution when the added lithium has been consumed by precipitation of hydrated lithium aluminate. Rodger et al. [11] suggested that the composition of the solution is in the region of supersaturation with respect to C_2AH_8, five minutes after mixing. This theory was directly related the influence of the C/A ratio on the supersaturation regions with respect to the CAC hydrates as it was already advanced by the theory of Barret et al. [14] on the induction period in CAC solution. Although the mechanism of acceleration by adding lithium sulphate is not investigated in detail in the present work, the consequences of this admixture on the microstructure of hydrated CAC paste are studied.

Finally this article presents new data on phase quantification as the determination of the degree of CA hydration measured by SEM Image Analysis and the porosity from Mercury Intrusion Porosimetry.

2. Materials and methods

2.1. Materials

The CAC reference was Secar 51 supplied by Kerneos (France). The oxide composition (from XRF analysis) and the quantification of crystalline phases (from XRD Rietveld analysis) are given in Tables 1 and 2 respectively. To control the setting time of CAC pastes, Li_2SO_4 was premixed with the water and added to the cement paste according $0.012\%_{wt}$ of the cement mass. The water to cement ratio (W/C) was 0.4 throughout. To prepare the cement paste, the powder was added to water and mixed with a paddle for 90 s at a speed of 1200 rpm.

2.2. Paste curing

The microstructural development of CAC depends strongly on the temperature. CAC hydration is an exothermic reaction releasing heat and leading to significant self heating even for small sections of cement paste. The reactions are not only exothermic but particularly rapid, so accurate control is challenging and poses specific experimental problems. To control temperature, a new experimental set up was developed [15]. The freshly mixed paste was cast in small copper moulds (38 mm diameter and 5 mm height). The moulds were sealed with grease and directly immersed in a thermostatically controlled water bath to maintain the paste temperature during hydration. For each set of experiments, one mould was equipped with a thermocouple to measure the temperature within the paste. The moulds were stored in a water bath for 24 h according to five time–temperature profiles, illustrated in Fig. 1: three isothermal regimes at 20 °C, 38 °C and 70 °C, a simulated self heating (SSH) input from a field test temperature profile (as measured in a 12 cm thick slab made of CAC concrete) reaching 50 °C as maximum temperature and a progressive ramp of 10 °C h^{-1} from 20 to 70 °C, to simulate the temperature profile possible in larger masses. For each discrete age of hydration up to 24 h, a mould was removed from the water bath and the cement hydration stopped as described in Section 3.3. After 24 h all the pastes, irrespective of earlier curing conditions, were demoulded and cured under water at 20 °C.

Table 2
Crystalline phases of CAC.

Crystalline Phases	CA	C_2AS	$C_{12}A_7$	Ferro perovskite	α-A	C_2S	Pleochroite (Phase Q)
% mass	63.5	21.5	0.4	5.0	3.0	2.1	4.2

2.3. Stopping of hydration

The main difficulty of a microstructural study of hydrated cement is to stop the chemical process at discrete times, without modifying the integrity of paste and the nature of the hydration products. In the case of CAC there is the additional challenge of stopping rapid reactions quickly. Two methods were applied: freeze-drying and solvent exchange. From the first minute up to 24 h, the freeze-drying method was chosen. The samples were immersed in liquid nitrogen for 5 min and placed in a freeze-dryer (Telstar Cryodos 50) for 24 h, at −50 °C temperature and 0.175 mbar vacuum, to sublimate the ice. The solvent exchange method was used from 24 h of hydration. The slices of paste were manually broken into pieces and then immersed in isopropanol for 6 days. They were then left for at least 2 days in a dessicator to allow the isopropanol to evaporate.

2.4. Isothermal calorimetry

Isothermal calorimetry is a simple method to study the kinetics of exothermic reactions occurring in controlled conditions and measures the heat flow in J h^{-1} g^{-1} of cement. Due to the ex-situ mixing of the cement paste, the first dissolution peak is not measured and only the energy due to subsequent hydration reaction is considered in the cumulative heat curves. The measurement was carried out using a TAM Air calorimeter and thermostat 3114/3236 from Thermometric. Five to ten grams of fresh cement paste were cast in a glass vial and a second vial of water (providing the same specific heat than the mass of cement paste) was used as a reference in the twin channel of calorimeter to ensure the stability of the baseline.

2.5. X-ray diffraction

Due to lack of knowledge on the detailed structures of non crystalline aluminium hydroxide but also of CAH_{10} and C_2AH_8, phase

Table 1
Oxides composition of CAC.

Oxides	CaO	SiO_2	Al_2O_3	Fe_2O_3	SO_3	MgO	K_2O	TiO_2	Na_2O	P_2O_5	Mn_2O_3	LOI
% mass	36.08	5.05	51.69	1.96	0.07	0.84	0.43	2.44	0.12	0.21	0.05	1.06

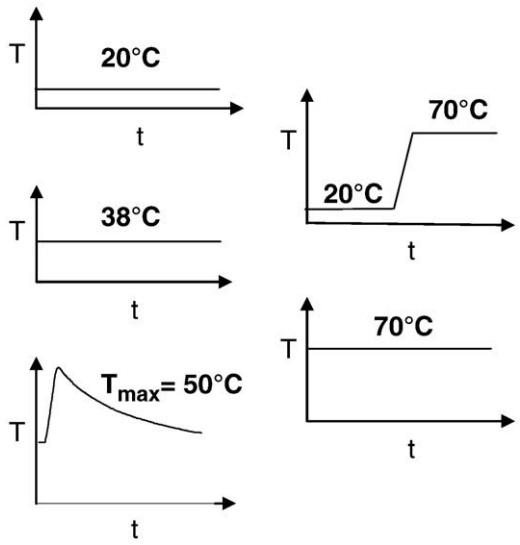

Fig. 1. Schemes of the time–temperature histories of cement pastes hydration for 24 h.

quantification by the Rietveld method cannot be easily used for CACs. Consequently a semi quantitative approach was used to determine the phase assemblage in each system, using the area under the main diffraction peak of each phase. Powder samples were preferentially used due to the small size of the samples removed from the water bath and the calorimeter. A dried sample was ground and sieved to 100 microns. The powder was then packed in a sample holder using an unpolished glass plate. XRD was carried out with an X'Pert Pro PANAlytical diffractometer (Cu tube, $\lambda = 1.54$ Å).

2.6. Scanning electron microscopy and image analysis

SEM can be used to study the development of microstructure. The local chemistry of phases present can be analyzed (with elementary analysis from energy dispersive spectroscopy) and the relative amounts of these phases can be quantified with backscattered electron image analysis (BSE-IA) on polished sections. A Philips Quanta 200 microscope with PGT energy dispersive X-ray analyzer was used, with an accelerating voltage of 15 kV. A novelty in this work is the use of backscattered electron image analysis (BSE-IA) technique for CACs. The method is based on the segmentation and the quantification of grey levels of each BSE image. The grey level of each phase is a function of the backscattering coefficient, which is related to the weight atomic averaged density Z. Fig. 2 shows three

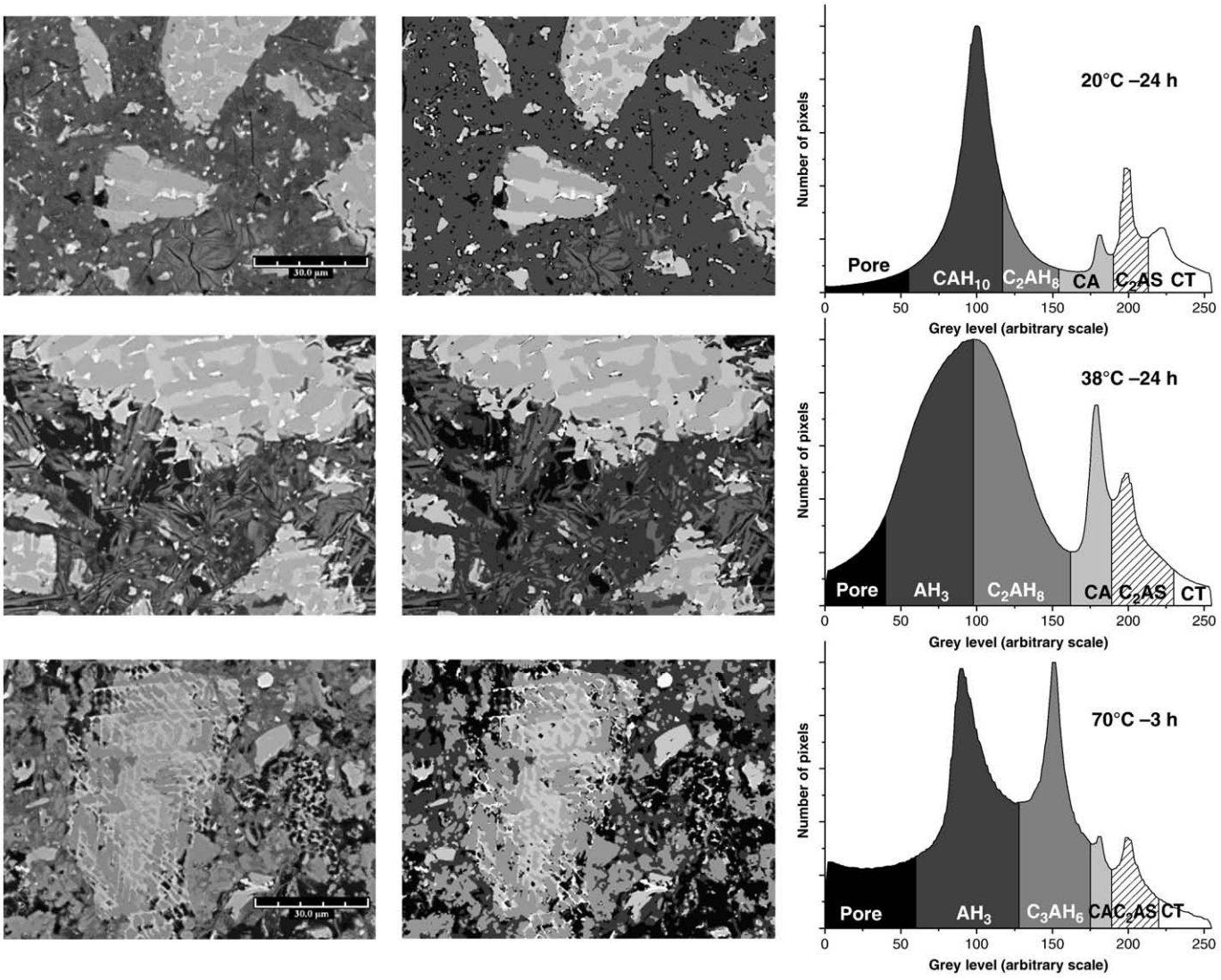

Fig. 2. Segmentation of BSE images for CAC hydrated at 20, 38 and 70 °C (left: original BSE image, middle: segmented image, right: histogram of grey levels segmentation).

examples of original images, segmented images and grey level histograms showing different phase assemblages. The grey level histograms are the cumulative histogram of a set of 300 BSE images, which were analyzed for each sample. The difficulty in differentiating the metastable phases from hydrated alumina is clear for the specimens cured at 20 and 38 °C. Consequently these hydrated phases cannot be accurately quantified. In the converted systems the histogram better differentiates C_3AH_6 from hydrated alumina. The results of BSE-IA are area fractions of each phase which are equal to the volume fraction. Regardless of the curing temperature, CA is well discriminated by BSE-IA and its degree of hydration (DH_{CA}) is determined by Eq. (6).

$$DH_{CA}(\%) = \frac{\%vol_{CA(t=0)} - \%vol_{CA(t)}}{\%vol_{CA(t=0)}}.100 \quad (6)$$

where $vol_{CA(t=0)}$ and $vol_{CA(t)}$ are respectively the initial volume of CA and its volume at time *t*.

For each age, only one sample (i.e. 300 images) is analyzed, the standard error of measurement ($sem_{(t)}$) for the CA volume and the consequent error in the degree of CA hydration (Δ_{DHCA}) are determined by Eqs. (7) and (8) respectively.

$$sem_{(t)}(\%) = \frac{\sigma}{\sqrt{N}} \quad (7)$$

$$\Delta_{DHCA}(\%) = DH_{CA}.\frac{sem(t)}{\left(\%vol_{CA(t=0)} - \%vol_{CA(t)}\right)} \quad (8)$$

where σ is the standard deviation over all images and N the number of images for each age.

2.7. Mercury intrusion porosimetry

Due to the complexity of the microstructural development, characterization methods for porosity are not well established for CAC based materials and very little data on MIP applied to CAC are available in literature [16–18]. Although MIP is a common technique to characterize the porosity of cementitious materials, it is very sensitive to sample preparation (e.g. sample size [19] or drying method [20]) and the interpretation of results is often controversial [21,22]. The porosimeter used was from Porotec equipped with two devices. The first applies low pressure of Hg up to 400 kPa to measure macroporosity and the second applies a maximum pressure of 400 MPa for the measurement of microporosity. To be comparable and to avoid the artefacts related to the drying method, both the 24 h and 90 d samples were dried by solvent exchange. For each analysis, two pieces of a cement paste slice (5 mm thick) were placed in the dilatometer cell. The slice was always fractured so that the pieces have only two smooth sides (which were in contact with the casting mould) and the rest of the pieces having fractured surfaces. This protocol was used to get comparable state of surface in contact with mercury during percolation. The total mass of sample was around 2 g. The contact angle was taken as 145° and a model of cylindrical pores was chosen. The measurement was done on two different samples and an error bar on the averaged total porosity is shown on Fig. 16.

3. Results

3.1. Hydration of CAC in isothermal 20 °C conditions

3.1.1. Isothermal calorimetry at 20 °C

The heat flow curves for the cement pastes without and with 0.012%$_{wt}$ Li_2SO_4 are shown in Fig. 3a and b respectively. The first exothermic signal, related to the initial dissolution of cement, decreases rapidly leading to a constant state generally termed *induction period*. During this period, it has been shown that the

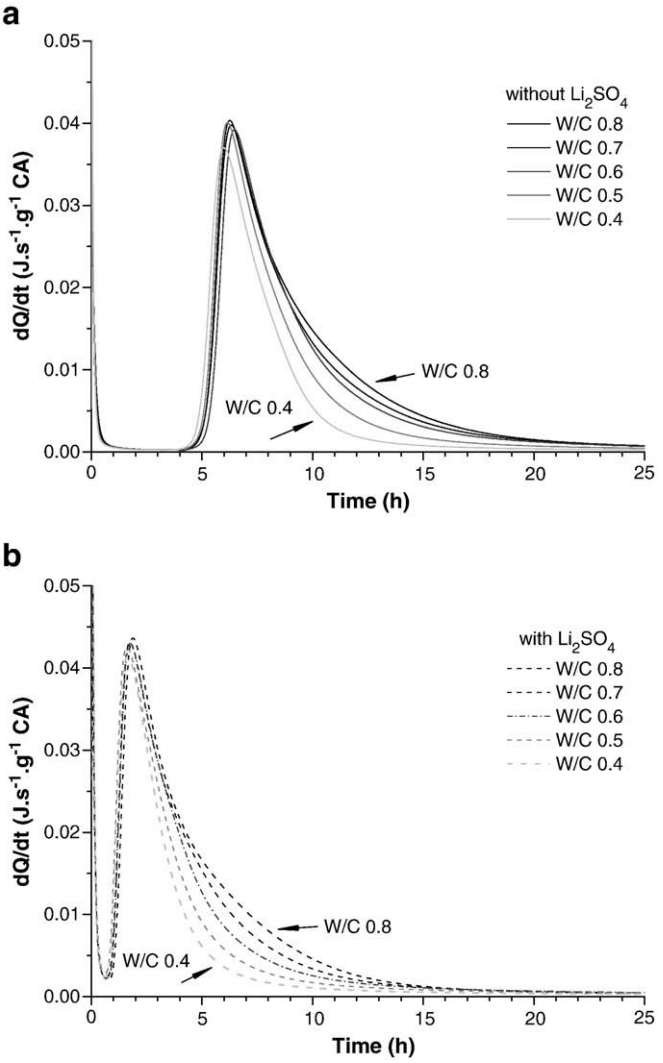

Fig. 3. Heat flow curve of CAC hydrated at 20 °C for different W/C ratios. a: without Li_2SO_4, b: with 0.012%$_{wt}$ Li_2SO_4.

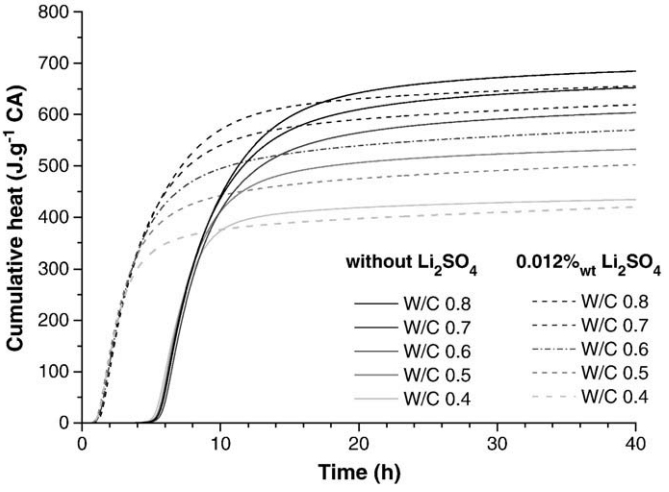

Fig. 4. Cumulative heat of CAC hydrated at 20 °C for different W/C, without and with 0.012%$_{wt}$ Li_2SO_4.

concentration of Ca^{2+} and $Al(OH)_4^-$ reaches a maximum level in the solution [11,14,23–26]. Then a single sharp peak occurs after 12 h of hydration corresponding to the massive precipitation of hydrates.

When Li_2SO_4 is added, the induction period is shortened and the calorimetric peak occurs after 1 h of hydration. From the cumulative heat curves (Fig. 4) it is observed that when Li_2SO_4 is added, the total heat, measured for different W/C ratios, is slightly lower than in the system without Li_2SO_4. This is consistent with the lower degree of hydration measured by BSE-IA (Table 4).

3.1.2. Phase assemblage at 20 °C by XRD

The qualitative XRD analysis is based on the area under the main diffraction peaks related to the anhydrous phases (30 and 31.4° 2θ respectively for CA and C_2AS) and hydrates (12.4, 8.7 and 31.3° 2θ respectively for CAH_{10}, C_2AH_8 and C_3AH_6). The evolution of the areas is compared with the heat evolved in the systems, illustrated by the dashed line on Fig. 5. The evolution of phases is very similar both without and with Li_2SO_4 systems. The consumption of CA slows down dramatically as soon as the main calorimetry peak ends, but still goes on at a low rate up to 280d. CAH_{10} predominates but a small amount of C_2AH_8 also precipitates without or with Li_2SO_4, as suggested by Rodger et al. [11]. The signal related to CAH_{10} increases significantly between 1 and 7 d curing but the consumption of CA remains very small. The change in drying methods (from freeze-drying to solvent exchange) must be considered as a reason for this sudden jump in the intensity related to CAH_{10}. The change from freeze-drying up to 24 h to solvent exchange at later ages, suggest that freeze-drying damages the crystallinity of CAH_{10}. The subsequent cure under water leads to the slow disappearance of the small amount of C_2AH_8 and the progressive formation of a very small amount of C_3AH_6 in the system containing Li_2SO_4. In the first hour of hydration, there is a small but significant drop in the main peak of C_2AS. This is most likely a dilution effect as the mass of the solid phase increases due to incorporation of water.

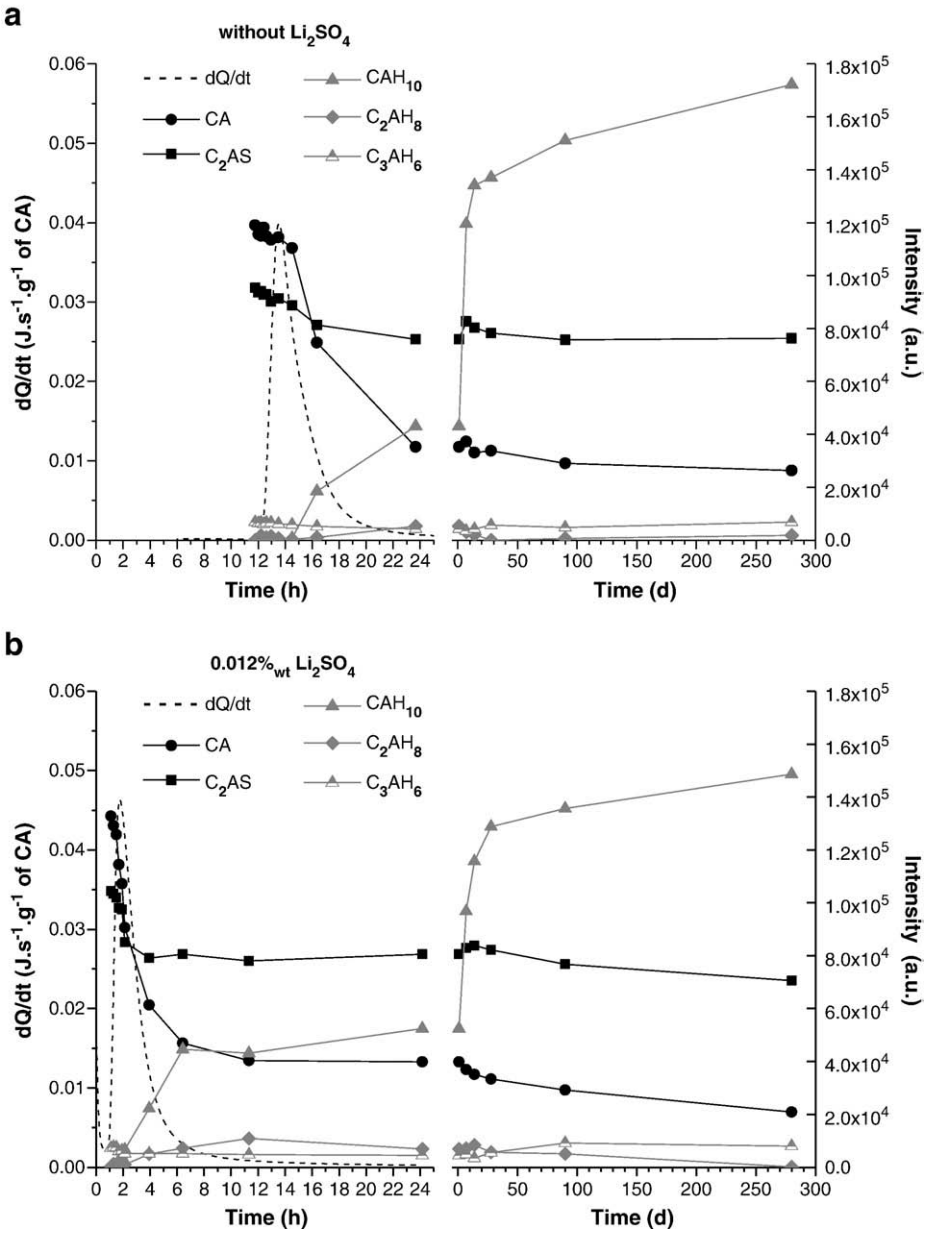

Fig. 5. XRD results of CAC hydrated at 20 °C, left y-axis and dashed line: calorimetric curve; right y-axis: area under diffraction peaks. a: without Li_2SO_4, b: with 0.012%$_{wt}$ Li_2SO_4.

3.1.3. SEM examination at 20 °C

From Fig. 6, the microstructural development looks similar in both systems with and without Li_2SO_4 after 24 h hydration and is dominated by CAH_{10}. However the number of C_2AH_8 plates in the pore space and at the boundary of the cement grains appears to be greater with Li_2SO_4 (Fig. 6-b), supporting the hypothesis of Rodger et al. [11] that Li_2SO_4 leads to the formation of AFm hydrates which promote the nucleation of C_2AH_8.

3.2. Hydration of CAC under 38 °C isothermal conditions

3.2.1. Isothermal calorimetry at 38 °C

Fig. 7 shows the heat flow curves obtained at 38 °C, for W/C = 0.4, without and with Li_2SO_4. As with hydration at 20 °C, the main reactions occur within the first hour of hydration. However the calorimetry at 38 °C shows significantly different reaction patterns according to the presence or not of lithium sulphate. Without Li_2SO_4, the hydration of CAC is characterized by a main peak followed by a second and less intense one, both occurring between 4 and 15 h. In contrast, adding 0.012%$_{wt}$ Li_2SO_4 leads to a single very rapid reaction ending by five hours. The microstructural development strongly differs from that seen at 20 °C. Fig. 7 shows the microstructure of the CAC paste without Li_2SO_4 after 7 h hydration at 38 °C (between the two consecutive calorimetric heat generation peaks) and reveals the difficulty of hydrate nucleation without admixture. Although the nucleation mechanism is heterogeneous in both cases, the distribution of the hydrates in space is more homogeneous in the case of Li_2SO_4 than in the case without where the distribution is very uneven.

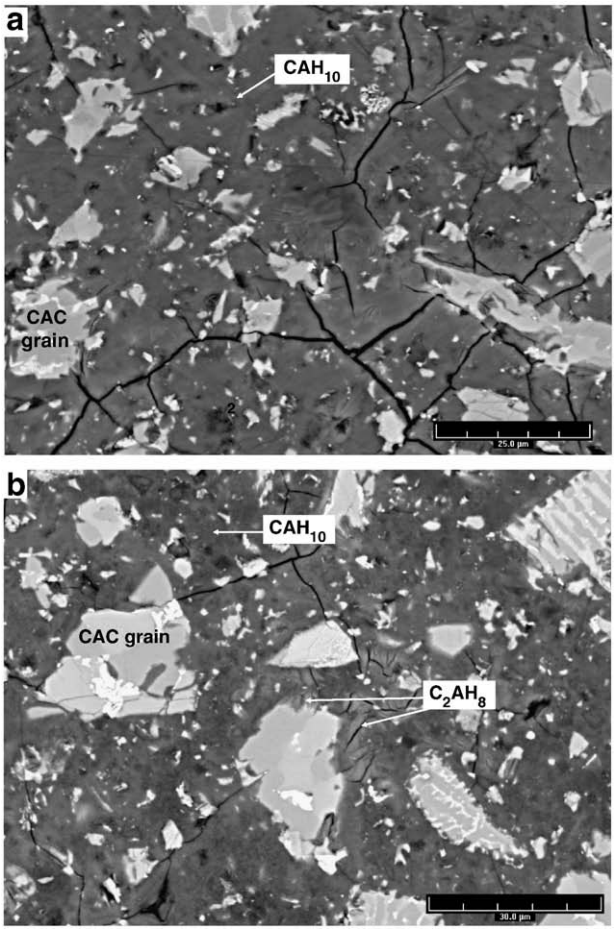

Fig. 6. Comparison of microstructure of Low-Fe CAC hydrated at 20 °C at 24 h. a: without Li_2SO_4, b: with 0.012%$_{wt}$ Li_2SO_4.

The total amount of heat evolved rapidly levels off (Fig. 7-c) and is greater in the systems without Li_2SO_4 after 10 h. The effect of Li_2SO_4 in lowering the overall heat evolved was already noted for 20 °C and could be attributed to the lower degree of CA hydration, as confirmed by BSE-IA (Table 4).

3.2.2. Phase assemblage at 38 °C by XRD

XRD analyses were carried out for the systems without and with Li_2SO_4. The temperature was constant at 38 °C for 24 h and then the paste is cured at 20 °C to be close to realistic curing conditions. Fig. 8 shows the evolution of the area under the main diffraction peaks. Due to the low crystallinity of aluminium hydroxide, the intensity of this phase is not shown. Here again the ongoing consumption of CA levels off as soon as the main calorimetry peaks ends, marking the time from which the signal related to C_2AH_8 is fairly constant up to 24 h. XRD analysis (Fig. 8) clearly shows that the second peak, measured in the systems without Li_2SO_4, corresponds to the precipitation of C_2AH_8 as suggested by SEM examination (Fig. 7-a). The dissolution of C_2AH_8 and the precipitation of C_3AH_6 are initiated from the first day of post curing at 20 °C, leading to a higher degree of CA hydration (than for initial curing at 20 °C) as more space and water are available for continued reaction. As for 20 °C, an initial drop in the main peak for C_2AS is observed that is attributed to the dilution of cement in water, as already explained in 4.1.2, but its consumption really starts during the later curing in water at 20 °C. According to the evolution of their respective peaks, the consumption of C_2AS can be correlated with the precipitation of C_2ASH_8 up to 180d.

In the paste with Li_2SO_4, C_2AH_8 precipitates rapidly and only one calorimetric peak is measured. The micrograph of Fig. 7-b shows the even precipitation of C_2AH_8 through the microstructure in presence of Li_2SO_4. Otherwise, the XRD patterns show similar trends in term of CA and C_2AS consumption during the water curing, but also on the evolution of C_2AH_8, C_3AH_6 and C_2ASH_8.

3.2.3. SEM examination at 38 °C

From the earliest age the space is almost filled with AH_3 and the plate-like hydrates (C_2AH_8), which predominate over 180d days of curing (Fig. 9). The composition of these plates was analyzed at 1 and 180 d by microanalyses. In the microanalyses, Fig. 10-a, the Ca/Al ratio varies from that of C_2AH_8 to that of AH_3. Silica is present as traces after 24 h, with the Si/Al ratio generally lower than 0.1 but significantly increases by 180 d, corresponding to the precipitation of C_2ASH_8. At this age, a hydrated phase is also observed appearing as dark patches in the cement grains (shown in Fig. 9-d), with a composition indicating an intermixing between C_2ASH_8 and C_3AH_6 (Fig. 10-b) in various proportions.

3.3. Hydration of CAC in simulated self heating conditions (SSH)

For these experiments, CAC paste was cured with a realistic time-temperature history. A temperature profile was recorded in a CAC 12 cm thick concrete slab in which the maximum temperature reached was 50 °C. This profile was used as input to control the water bath, in order to simulate and impose a comparable self heating on the cement paste. The same profile of temperature was used for the systems without Li_2SO_4, without taking account of the longer induction period initiated by the absence of accelerator.

3.3.1. Phase assemblage in SSH conditions by XRD

The XRD results are shown in Fig. 11. The phase assemblage at less than 24 h was studied only for the cement pastes containing Li_2SO_4. In the hydration at 20 and 38 °C, the reaction of CA levelled off after the main calorimetric peak. During the self heating of cement paste, the hydration of CA levelled off when the maximum temperature was reached. From this point the signals related to C_2AH_8 and C_3AH_6 were constant up to 24 h. As observed for the hydration at 38 °C, dissolution

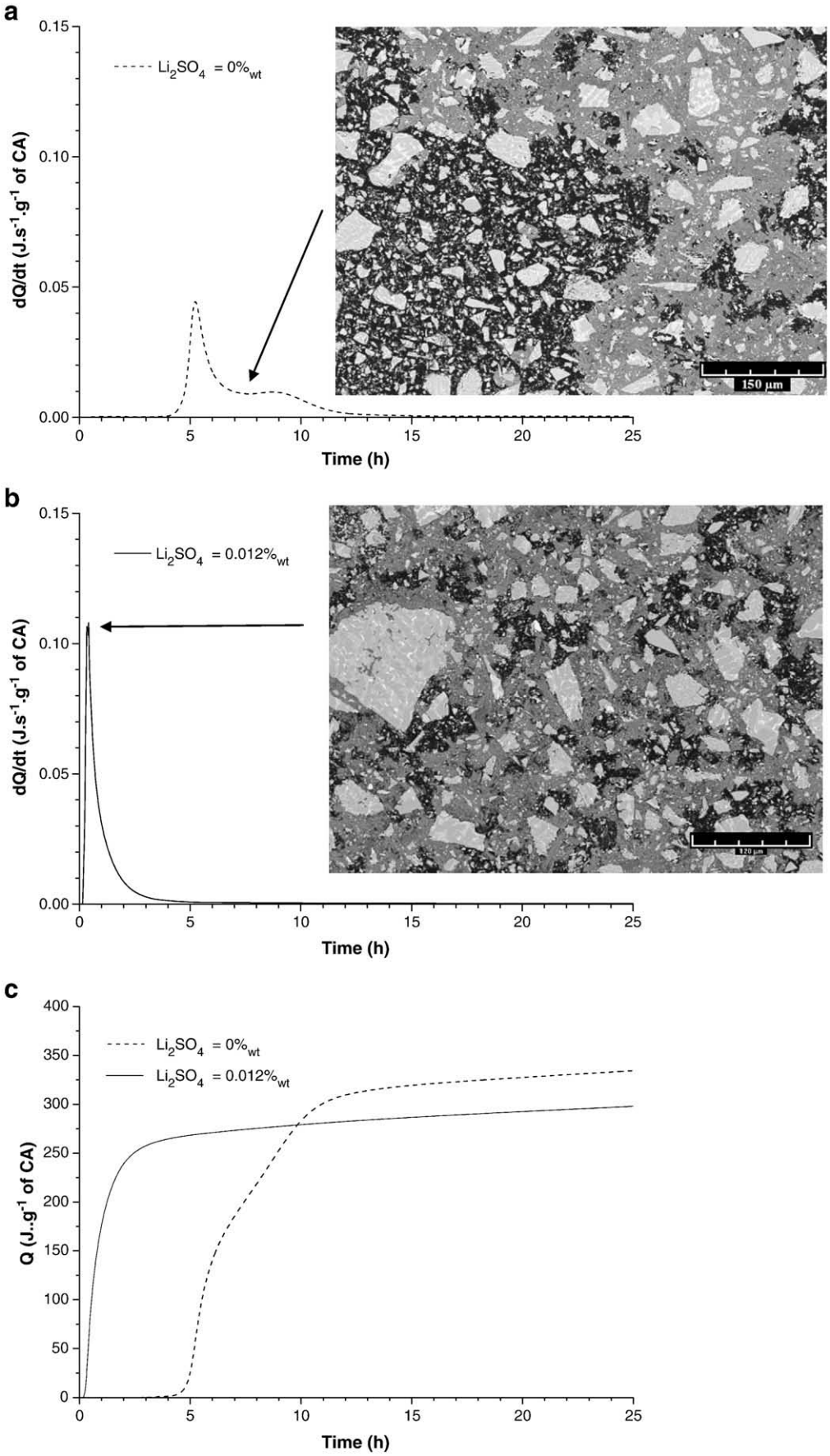

Fig. 7. Isothermal calorimetry and SEM micrographs of CAC hydrated at 38 °C, a: heat flow curve without Li_2SO_4; b: heat flow curve with 0.012%$_{wt}$ Li_2SO_4; c: cumulative heat curves.

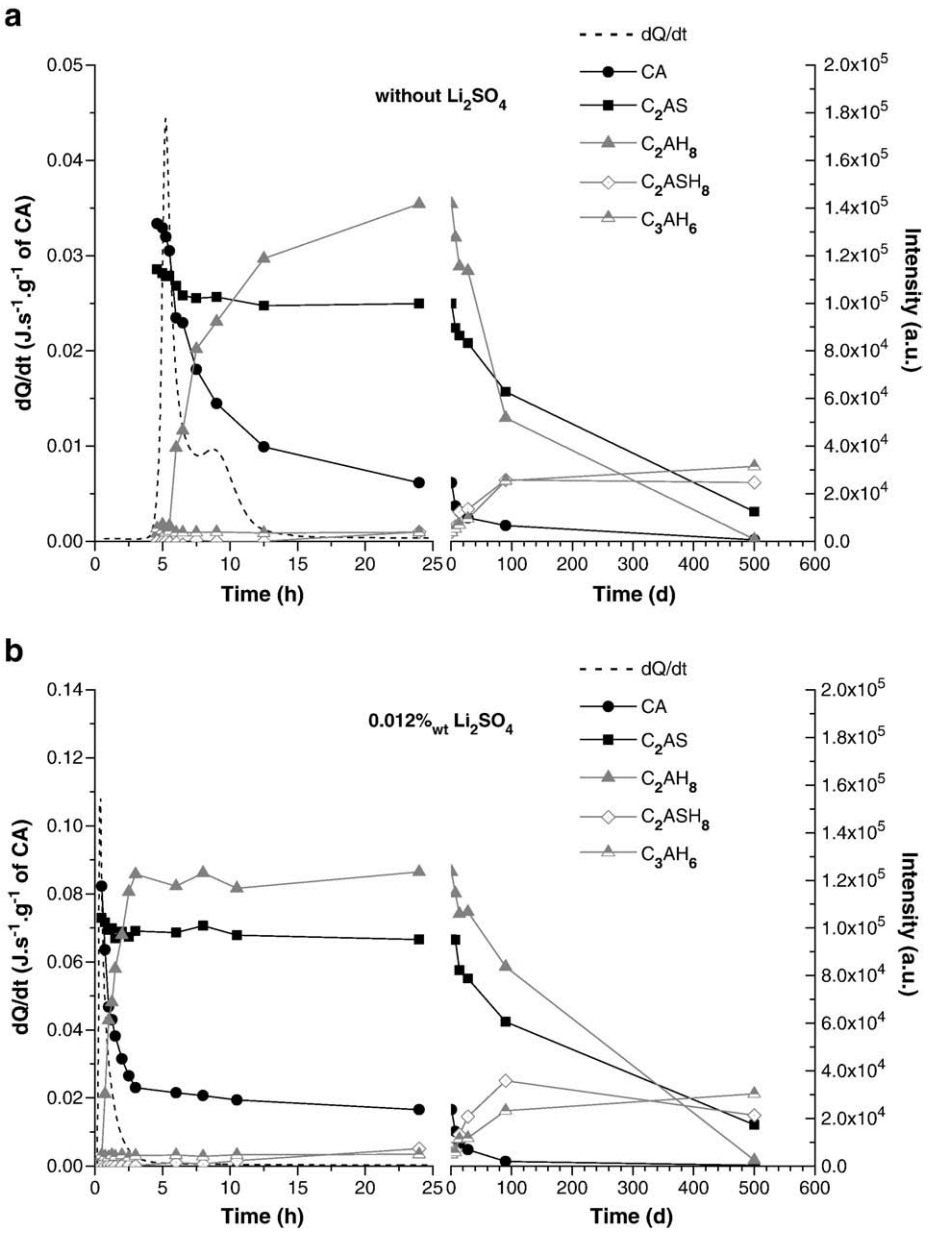

Fig. 8. XRD results of CAC hydrated at 38 °C, left y-axis and dashed line: calorimetric curve; right y-axis: area under diffraction peaks. a: without Li_2SO_4; b: with 0.012%$_{wt}$ Li_2SO_4.

of C_2AH_8 occurs during the subsequent 20 °C curing but the addition of Li_2SO_4 significantly modifies the kinetics: as the dissolution of C_2AH_8 is significant from 7d in the paste with Li_2SO_4, but only from 28d without Li_2SO_4. The progressive decrease of the signal related to C_2AH_8 can be attributed to the precipitation of both C_3AH_6 and C_2ASH_8. The latter can also be related to the hydration of C_2AS with becomes significant during the 20 °C curing. As well as changing the kinetics of C_2AH_8 dissolution Li_2SO_4 also favours the precipitation of C_3AH_6 rather than C_2ASH_8 compared to the system without Li_2SO_4. Finally, a very small amount of CAH_{10} is detected at 90 d in the systems containing Li_2SO_4, which was not observed with the hydration at isothermal 38 °C (Fig. 8).

The development of the microstructure under these conditions of hydration seems very similar to that developed under 38 °C isothermal conditions. However self heating conditions and the extra temperature rise to 50 °C may influence the early age growth of C_2AH_8 and AH_3 phases and subsequent space filling as discussed in 4.6.

3.4. Hydration of CAC at 70 °C

Two different time–temperature histories were applied to study the influence of the progressive heating on the assemblage of C_3AH_6 and AH_3. The cement paste was placed in a water bath at 70 °C immediately after mixing and casting (around 10 min) or progressively heated up to 70 °C, using a ramp of 10°/h from 20 to 70 °C from the end of the induction period (measured in parallel by calorimetry). For these time–temperature histories, only the results on cement paste containing 0.012%$_{wt}$ Li_2SO_4 are presented as it was not possible to well control the setting time and heating without Li_2SO_4.

3.4.1. Phase assemblage at 70 °C by XRD

The phase assemblages measured by XRD are shown in Fig. 12-a and b. Here the better crystallinity of AH_3 allows it to be plotted, using the diffraction peak related to the [002] plane (at 18.27° 2θ). For such a temperature, the hydration is very rapid and all CA is consumed

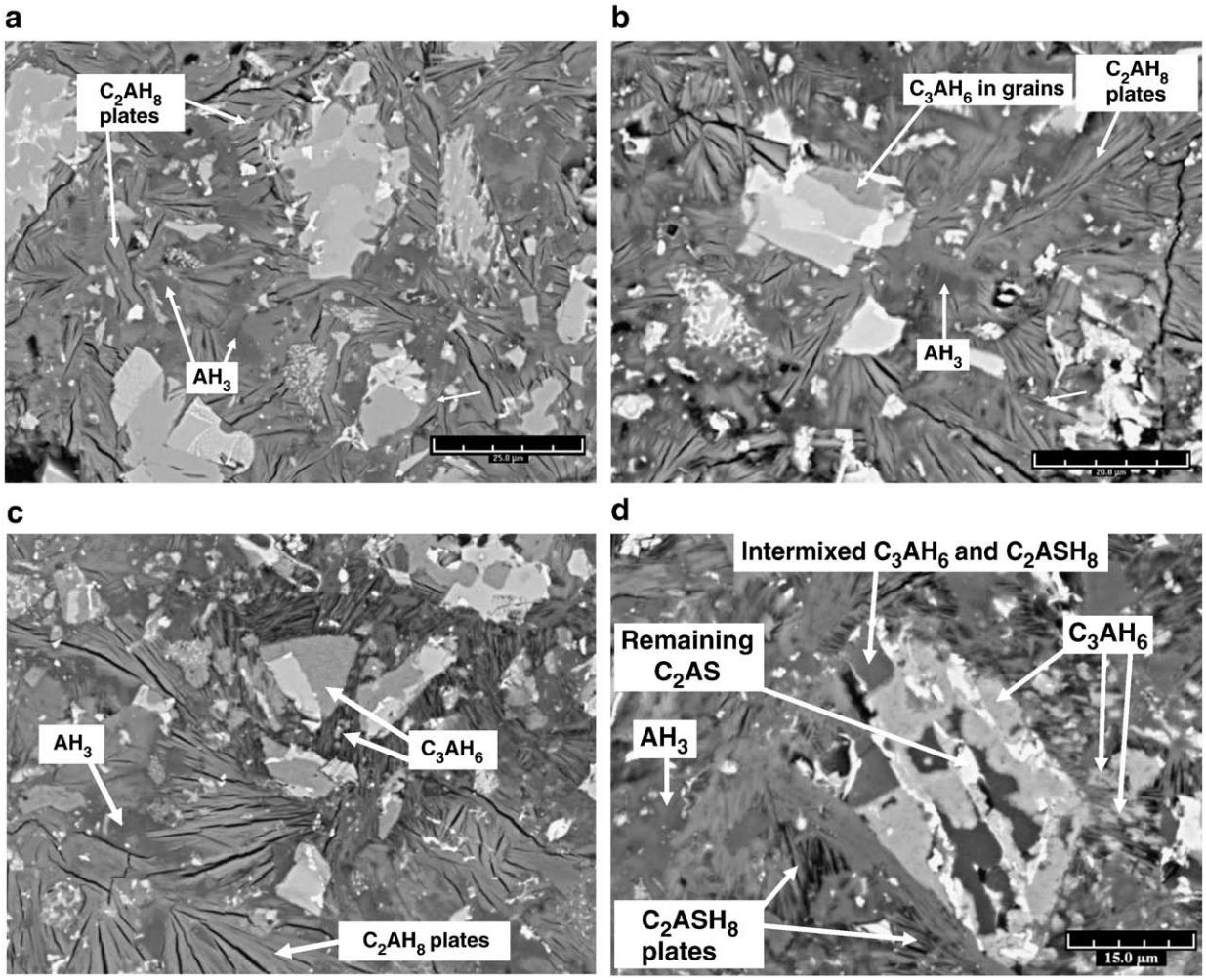

Fig. 9. SEM micrographs of CAC hydrated in isothermal 38 °C for 24 h. a: 24 h without Li_2SO_4; b, c and d: 24 h, 90 d and 200 d with 0.012%$_{wt}$ Li_2SO_4.

after 3 and 6 h, respectively for the direct immersion at 70 °C and the ramp.

In the first condition (Fig. 12-a), the precipitation of C_2AH_8 is instantaneous and the maximum intensity is measured after 0.5 h. At that age a small amount of C_3AH_6 is already detected. The amount of C_2AH_8 decreases rapidly up to 3 h, marking the time from which the amount C_3AH_6 and AH_3 stays constant up to 360d. For hydration with the temperature ramp (Fig. 12-b), the precipitation of C_2AH_8 is progressive up to 5 h, when the temperature applied to the paste is 60 °C. Then C_2AH_8 dissolves rapidly and C_3AH_6 starts to precipitate. Under both conditions, AH_3 precipitates initially with C_2AH_8 but its amount increases significantly during the precipitation of C_3AH_6. In parallel, the consumption of C_2AS already starts during the hydration at 70 °C and continues slowly during the cure at 20 °C under water.

Regardless of the time–temperature history leading to 70 °C, the early age precipitation of siliceous hydrogarnet, as solid solution of C_3AH_6 [27], is detected by the XRD. The diffraction peak of this phase is characterized by a small shoulder well identified at high Bragg angles. Siliceous C_3AH_6 was mainly located by SEM-EDS in the cement grains and the substitution of aluminium by silica in the lattice of C_3AH_6 may results from the interaction between C_2AS and the precipitating C_3AH_6.

It is interesting to note that, from an early age, the signal related to AH_3 precipitation is lower in the case of the ramp than in the case of hydration at directly at 70 °C. Fig. 13 shows a typical XRD pattern of the pastes hydration for 24 h in both conditions, which further indicates that AH_3 has a different crystal structure according to the time–temperature history applied during its formation. The identification of the exact polymorphs requires caution, as both gibbsite and bayerite could fit with the respective diffraction patterns. Regardless of the conditions of hydration, both polymorphs precipitate but the formation of bayerite is more prominent in the paste directly hydrated at 70 °C.

3.4.2. SEM examinations of samples hydrated at 70 °C

Fig. 14-a and c show the microstructure of two samples after 0.5 h hydration at 70 °C and 4 h hydration with the ramp (when the paste temperature is 60 °C), for which the degree of CA hydration is 80 and 75% respectively (see Section 3.5). Fig. 14-a and c illustrate the difference in the morphology of C_2AH_8 and AH_3, and subsequent space filling. After 0.5 h at 70 °C, C_2AH_8 plates predominate in the pore space and inside the cement grains. The small amount of C_3AH_6 detected by XRD is not easy to identify. The ramp to 70 °C allows the progressive precipitation of C_2AH_8 and AH_3 which are well differentiated from each other. The C_2AH_8 plates look denser and space filling by aluminium hydroxide is especially clear in the case of the temperature ramp.

Later on, Fig. 14-b and d shows the microstructure after 3 h hydration at 70 °C and after 6 h hydration with the ramp respectively. These microstructures correspond to the minimum intensity of the

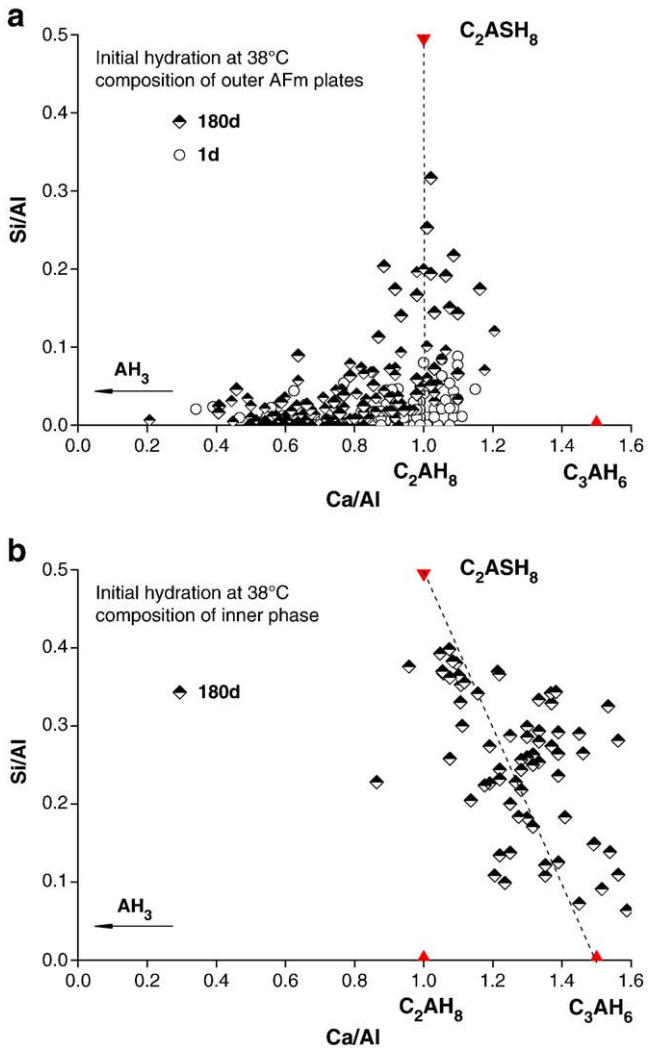

Fig. 10. Microanalysis of the AFm phases in the samples initially hydrated at 38 °C for 24 h. a: evolution of the outer AFm plates during the curing, b: composition of the inner phase after 180d curing.

XRD signal related to C_2AH_8 and the maximum signal related to C_3AH_6 and AH_3. The clusters of C_3AH_6 are located in the matrix, as well as on the edge of the dissolving C_2AH_8 plates, rather than just in the cement grains, replacing CA and adjacent to C_2AS, as seen for hydration at 38 °C and with SSH. As observed at earlier ages the microstructure of the paste hydrated with the ramp is denser. The difference in the densification of matrix according to the time–temperature history to 70 °C explains the difference in porosity reported below in Section 3.6.

3.5. Degree of CA hydration with different time–temperature histories

The preparation of polished sections, for early age SEM examinations, requires a good cohesion of the cement paste. Without accelerator, the induction period of this system can vary significantly and the cement can remain relatively soft for several hours. Consequently SEM examinations and BSE image analysis were mainly carried out on the systems containing Li_2SO_4 but a comparison was made for the system without admixture at 24 h (Table 4). The degree of CA hydration (DH_{CA} in Fig. 15) was measured for the different conditions of hydration according to the protocol described in Section 2.6.

From Fig. 15 it can be seen that the degree of CA hydration is highly dependent on the time–temperature history of the cement paste during the first day of hydration. To interpret the evolution of DH_{CA} in the different systems (containing 0.012%$_{wt}$ Li_2SO_4), Table 3 summarizes the phase assemblage after 24 h hydration and throughout the curing under water at 20 °C.

At 20 °C, 65% CA is consumed after 24 h in sealed conditions. During the subsequent curing under water, DH_{CA} increases progressively up to 85% at 90d and stays constant afterwards. This extra hydration could correspond to the further precipitation of CAH_{10} and C_3AH_6 as already suggested by the XRD (Fig. 5). Both 38 °C and self heating for which C_2AH_8 and AH_3 predominate have a comparable DH_{CA} after 24 h (respectively 80 and 85%). During the curing, XRD suggested that C_2AH_8 disappears progressively up to 90 d. Therefore the increase of DH_{CA} up to 85% is not linked to the formation of this phase but rather to the precipitation of C_3AH_6, which was mainly located instead of CA in the cement grains. Note that the initial self heating of the paste leads to a slower consumption of CA during the curing after 24 h. This could be linked to a difference in the matrix densification as it is suggested below by MIP results. In the systems hydrated at 70 °C for 24 h, the complete consumption of CA is measured after 3 and 6 h but with different kinetics, i.e. more rapidly for the hydration directly at 70 °C.

The influence of adding Li_2SO_4 on DH_{CA} after 24 h hydration at 20, 38 °C and self heating, is shown in Table 4. It is seen that a small addition of Li_2SO_4 limits the degree of CA hydration in all curing conditions, in agreement with the lower heat of hydration measured by calorimetry in pastes containing Li_2SO_4 (Figs. 4 and 7-c).

3.6. Development of porosity

MIP analysis was carried out on solvent exchanged cement pastes after 1 d of hydration and 90 days of curing under water at 20 °C (Fig. 16). After 1 d hydration, the total porosity and the pore size distribution are clearly distinguished according to each assemblage of hydrates.

As expected, the systems dominated by CAH_{10} have the finest porosity, i.e. the smallest pores and a total porosity of 16 to 17%vol. At 38 °C, the total porosity is slightly higher than that measured for hydration at 20 °C. The porosity of the self heated cement paste is noteworthy. Compared to the hydration at 38 °C, the total porosity is much higher and close to that measured in the paste progressively hydrated to 70 °C. This highlights the influence of the self heating on the assemblage of hydrates. Although the amount of C_2AH_8 and AH_3 is comparable to the 38 °C sample for both conditions of hydration, the assemblage is different in the self heated paste and has higher porosity. The porosity measured in the pastes hydrated at 70 °C confirms that the ramp to 70 °C leads to smaller breakthrough diameter and lower total porosity, resulting from the different space filling with lower density AH_3.

After 90 d curing under water, both total porosity and pore size decrease regardless of the initial temperature of hydration. In the system hydrated at 20 °C and dominated by CAH_{10}, there is no longer a clear breakthrough diameter after 90 d curing under water and the total porosity reaches a very low value of 3%. The test was repeated on samples cured for 90 and 300 d under water, and similar results were found. This indicates that the space is effectively completely filled by the precipitation of CAH_{10} between 1 and 90 d curing under water. However this low value of porosity could also reveal the limitation of MIP applied to such a dense microstructure.

When $C_2AH_8 + AH_3$ predominate after 24 h (38 °C isothermal and simulated self heating), the breakthrough diameter and the total porosity are decreased significantly after 90 d curing. However XRD results (Fig. 8) indicate that C_2AH_8 dissolved continuously and that both C_3AH_6 and C_2ASH_8 precipitated progressively. The conversion of C_2AH_8 to C_3AH_6 and AH_3 at a constant degree of hydration creates

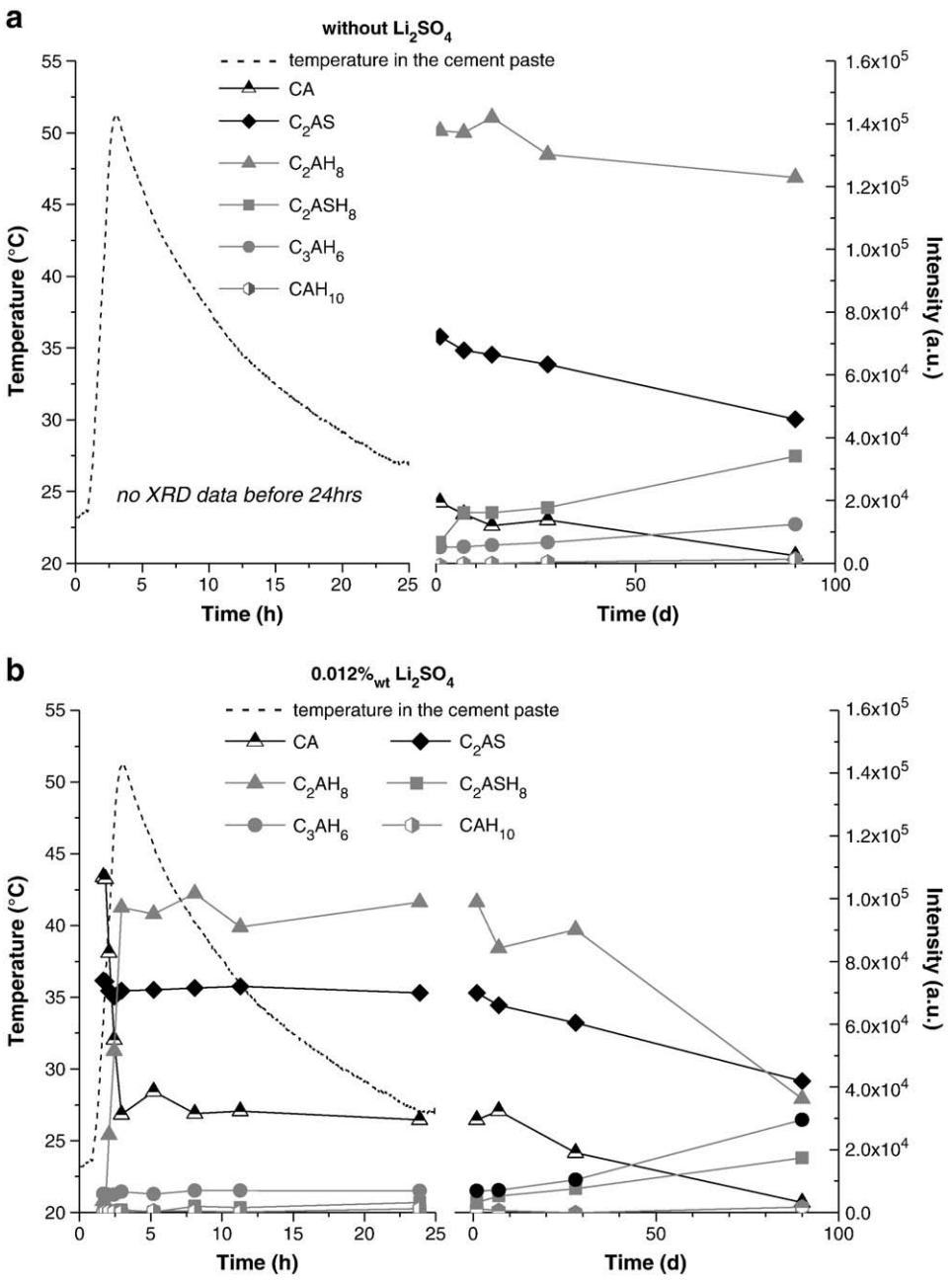

Fig. 11. XRD results of CAC hydrated in SSH conditions, left y-axis and dashed line: temperature profile in the cement paste; right y-axis: area under diffraction peaks. a: without Li_2SO_4; b: with 0.012%$_{wt}$ Li_2SO_4.

porosity, so the decrease must be due to the hydration of C_2AS and the formation of C_2ASH_8.

The main difference between the systems dominated by $C_3AH_6 + AH_3$ lies in the early precipitation of AH_3 with different crystal structures and density. The lower density AH_3 (identified as gibbsite) precipitates when the paste is heated up with the ramp while higher density AH_3 is identified as bayerite for the straight 70 °C curing. This explains the difference in the pore size distribution and total porosity measured after 24 h hydration. Later on both the total porosity and the threshold diameter decrease during the curing under water. The progressive formation of C_2ASH_8 and the small amount of extra AH_3 (suggested by XRD in Fig. 12) contribute to subsequent space filling as the amount of C_3AH_6 is stable and CA fully hydrated.

4. Discussion

This study gives new details about the microstructural development of CAC hydrated with different time–temperature histories, the influence of the self heating and the addition of Li_2SO_4 on the phase assemblage and the mechanisms of C_2AS hydration into C_2ASH_8.

4.1. Early age hydration of CAC

The experimental approach used in this work allowed the study of three phase assemblages CAH_{10}, $C_2AH_8 + AH_3$ and $C_3AH_6 + AH_3$, from the early minutes of hydration to several months of curing under water. The development of these assemblages rapidly levels off after a

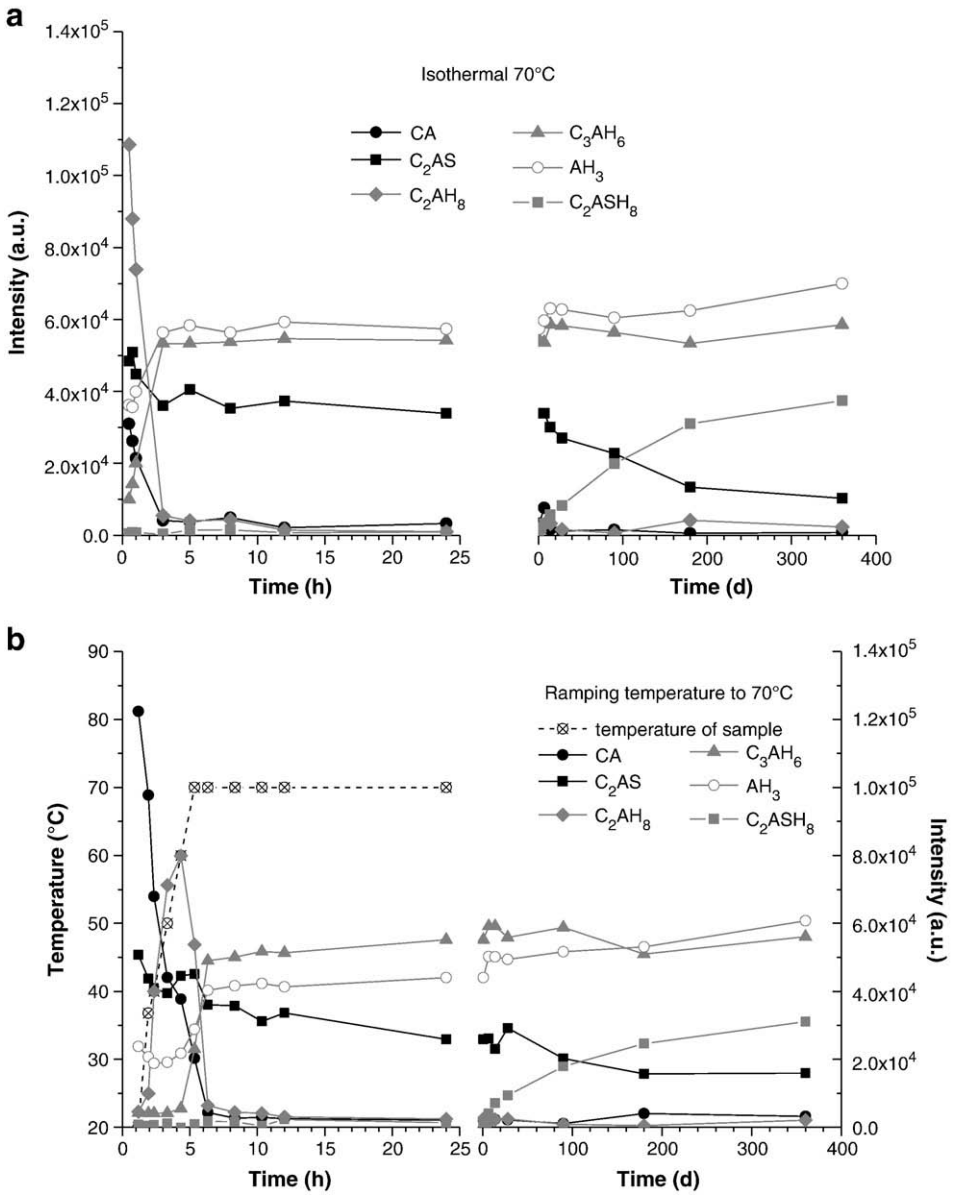

Fig. 12. XRD results of CAC, with 0.012%$_{wt}$ Li_2SO_4. a: hydration at 70 °C for 24 h, b: hydrated with ramp to 70 °C for 24 h (left y-axis: temperature in the paste; right y-axis: XRD intensity).

few hours of hydration and the reasons for the limitations of further hydration can be the lack of water, the lack of space or the lack of reactant. We can eliminate the last of these for the CAH_{10} and $C_2AH_8 + AH_3$ assemblages as there is clearly substantial CA left at the end of the main calorimetric peak (Figs. 5, 8 and 11). However for the $C_3AH_6 + AH_3$ assemblage, the reactant CA is exhausted during this period (Fig. 12). The question of whether the limiting factor for hydration is the lack of space or water was raised from the first results of calorimetry at 20 °C (Fig. 3a and b). From these experimental results it was not possible to discriminate these two factors. However Ideker [28] recently studied the early age properties of CACs materials and more precisely the chemical shrinkage occurring during hydration in isothermal conditions. In his experimental set up, the cement was cast in a plastic vials and covered by a small volume of water. The maximum magnitude of chemical shrinkage, related to the massive precipitation of hydrates at 20 and 38 °C, is rapidly reached and then followed by a steady signal. This supports the assumption that water is not the limiting factor for hydration, as an excess of water is available in this system. It indicates that space availability rather is the factor controlling the kinetics of hydration. Nevertheless in all cases the MIP results (Fig. 16) show that space is not completely filled at the end of the main heat generation peak. Even at 20 °C slow hydration continues over several months with consequent densification of the matrix. With C_2AH_8 as the main hydrate there is more space left between the plates which is later filled by other hydrates; and in this case appears to allow the hydration of C_2AS into C_2ASH_8. The hypothesis on the limiting factor of hydration kinetics by availability of space requires further investigation using cementitious micro-structure model as *μic* developed by Bishnoi [29]. This versatile platform model will provide an effective tool to study the reaction mechanism and growth and overlap processes of CAC hydrates.

4.2. Influence of self heating on the phase development

The experimental approach allowed the study of phase assemblage in CAC paste with self heating conditions of hydration. This approach

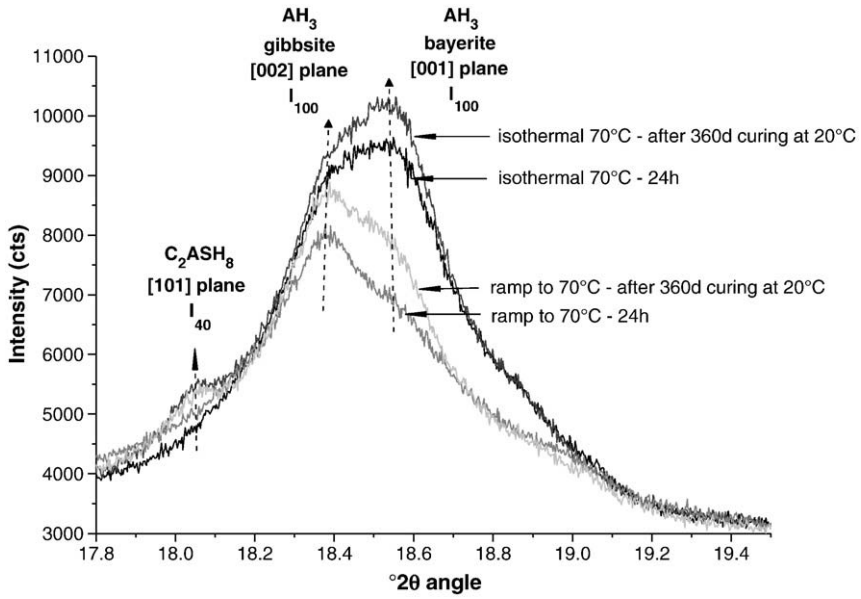

Fig. 13. XRD pattern of AH_3 in CAC paste hydrated for 24 h at 70 °C (isothermal and ramp) and after 360 d curing under 20 °C water.

revealed interesting results on the structural development of AH_3 during the formation of the stable assemblage $C_3AH_6 + AH_3$. It was shown that the temperature ramping to 70 °C favoured the precipitation of a lower density AH_3 compared to that precipitated during the isothermal 70 °C hydration. This difference in the density of AH_3 was supported by different methods (BSE-IA XRD) and led to the

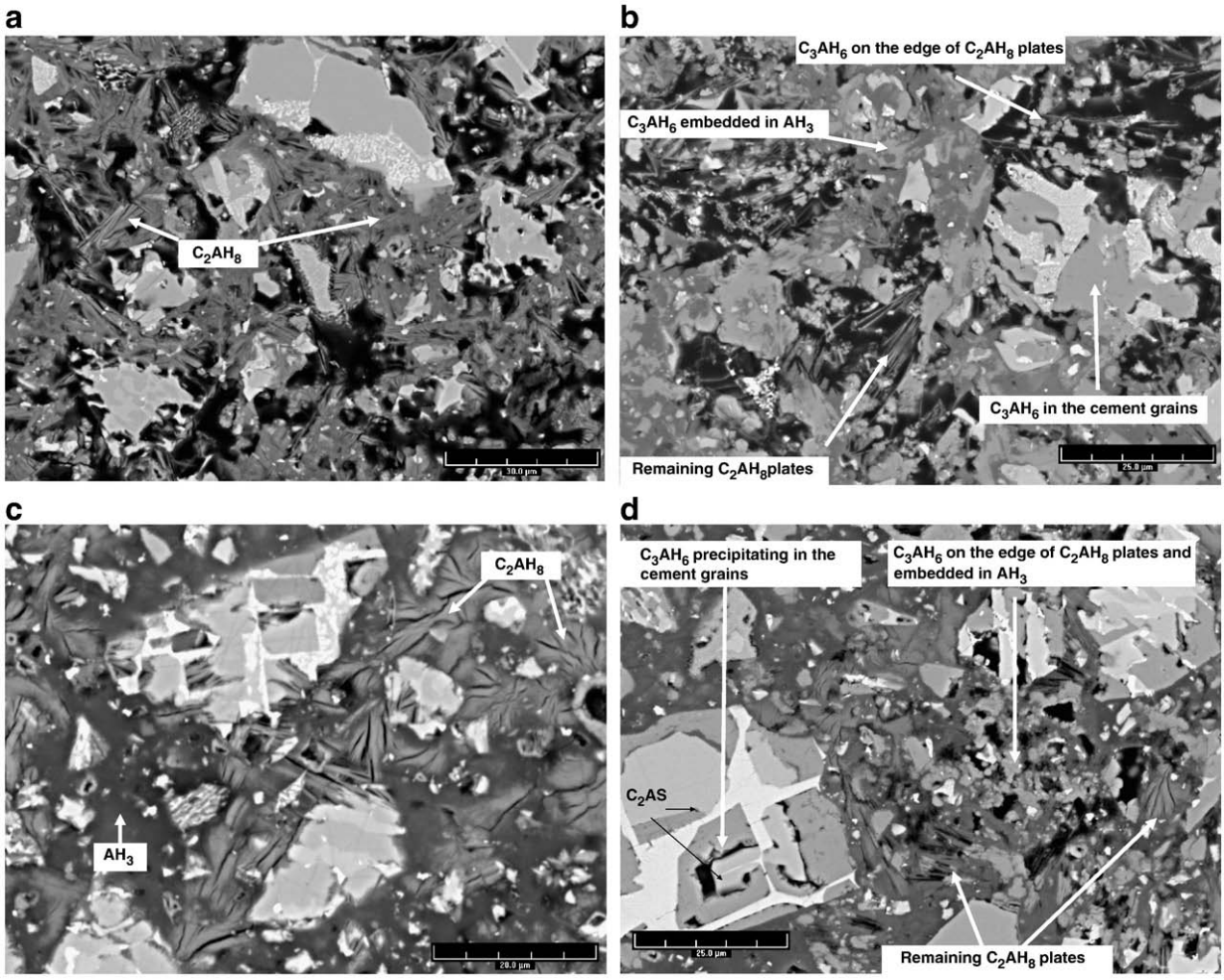

Fig. 14. SEM micrographs of CAC hydrated in isothermal 70 °C (a: 0.5 h and b: 3 h) and using the ramp (c: 4 h and d: 6 h).

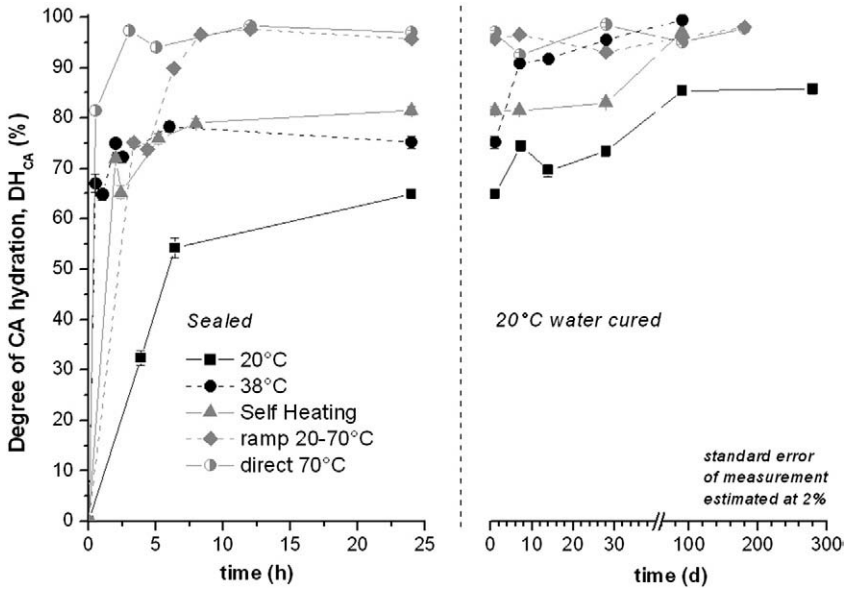

Fig. 15. Degree of CA hydration with different time–temperature histories, with 0.012%$_{wt}$ Li_2SO_4.

enhancement of space filling in self heated paste (lower porosity from MIP analyses). AH_3 has three crystalline polymorphs [30]: nordstrandite, bayerite and gibbsite, the later being the structure most reported in the literature on CAC hydration. However the present results indicate that gibbsite and bayerite co-precipitate in CAC paste according to the time–temperature history leading to the formation of the stable assemblage. The co-crystallization of gibbsite and bayerite can take place since they differ mainly in the manner of stacking or superposition of successive dioctahedral $Al(OH)_3$ layers [31]. Nevertheless, the full details of this process are not yet clear at present.

The other interesting results concern the difference in the space filling between the isothermal 38 °C and the simulated self heating conditions. In both cases, the hydration leads to the precipitation of comparable amounts of $C_2AH_8 + AH_3$. However the self heating up to 50 °C seems to limit the extend of the C_2AH_8 plates growth and produces less space filling after 24 h hydration than in isothermal 38 °C conditions (Fig. 16). However this available space leads to the further hydration of CA into a small amount of CAH_{10} during 90 days curing under 20 °C water, which strongly contributes to the matrix densification and the significant decrease of the porosity.

4.3. Formation of C_2ASH_8 in plain CAC systems

In CAC based systems, stratlingite C_2ASH_8 is a stable phase generally attributed to the interaction between metastable hydrates CAH_{10} and C_2AH_8 and reactive silica from SCMs such as slag, fly ash or silica fume. However the formation of C_2ASH_8 from C_2AS was clearly identified by XRD and SEM-EDS in the plain CAC system. Starting from the first day of hydration, the subsequent reactions (always at 20 °C) seem to be dependent on the phase assemblage either due to effects on nucleation or space available:

- In the CAH_{10} dominated systems, the hydration of C_2AS remains very slow and seems to be controlled by the lack of space.
- In contrast, for the assemblage $C_2AH_8 + AH_3$, the precipitation of C_2ASH_8 seems to be favoured. The presence of silica in the C_2AH_8 plates could indicate that C_2ASH_8 precipitates during the first hour of hydration. C_2AH_8 phase was characterized by a Si/Ca ratio remaining initially low, i.e. 0.2, but tending towards the stoichiometric value (0.5) during the water curing. It was shown that the progressive precipitation of C_2ASH_8 does not prevent the formation of C_3AH_6 but seems to control space filling and contributes to the decrease of porosity.
- Finally during the formation of the assemblage $C_3AH_6 + AH_3$, it appears that part of C_2AS reacts to form small amounts of Si-rich C_3AH_6 in the cement grains but most of it hydrates into C_2ASH_8 filling the porosity during the curing under water.

Regardless of the initial time–temperature history, the long term hydrated cement grains show the presence of inner C_2ASH_8 intermixed with C_3AH_6.

Table 3
Summary of the phase assemblage in the systems containing 0.012%$_{wt}$ Li_2SO_4.

Hydration up to 24 h	Phase assemblage identified at 24 h (with 0.012%$_{wt}$ Li_2SO_4)	Evolution of phase assemblage identified throughout the curing under water at 20 °C
20 °C	CAH_{10}	Progressive precipitation of small amount of CAH_{10},
	Small amount of C_2AH_8	Slow dissolution of C_2AH_8
		Slow precipitation of C_3AH_6 and C_2ASH_8
38 °C	$C_2AH_8 + AH_3$	Progressive dissolution of C_2AH_8
	Small amount of C_3AH_6	Progressive precipitation of C_3AH_6 and C_2ASH_8
Self heating	$C_2AH_8 + AH_3$	Progressive dissolution of C_2AH_8
	Small amount of C_3AH_6	Progressive precipitation of C_3AH_6 and C_2ASH_8
Ramp to 70 °C	$C_3AH_6 + AH_3$	Progressive precipitation of C_2ASH_8
70 °C	$C_3AH_6 + AH_3$	Progressive precipitation of C_2ASH_8

Table 4
Influence of 0.012%$_{wt}$ Li_2SO_4 on the degree of CA hydration after 24 h hydration at different temperatures.

Hydration condition for 24 h	20 °C	38 °C	Self heating
DH_{CA} without Li_2SO_4	77.9 ± 1.0%	88.1 ± 1.0%	84.4 ± 0.6%
DH_{CA} with 0.012%$_{wt}$ Li_2SO_4	65.0 ± 0.9%	80.6 ± 1.2%	81.5 ± 0.9%

4.4. Effect of Li_2SO_4 on the microstructure of CAC

The mechanism of hydration acceleration by Li_2SO_4 was not investigated in detail in this study. However, the formation of lithium aluminate hydrate suggested by different authors [10,11] was not observed for the Li_2SO_4 dosage used in this work, i.e. 0.012%$_{wt}$ Nevertheless the present results showed the consequence of the addition of Li_2SO_4 on the microstructure development of CACs systems. First of all the nucleation of hydrates is strongly enhanced by Li_2SO_4. This was particularly well observed at 38 °C for which the distribution of C_2AH_8 and AH_3 is very uneven without lithium sulphate (Fig. 7-a). In addition, the presence of Li_2SO_4 enhanced the precipitation of more stable hydrates and these products were detected from the first hours of hydration.

It might be expected that the consumption of CA should increase in presence of Li_2SO_4 due to the precipitation of the more stable products. In contrast, it was found that the addition of Li_2SO_4 noticeably decreases the final degree of CA hydration, as identified by the calorimetric results at 20 and 38 °C and the quantification of CA by BSE-IA. At present the reasons for this effect are not clear.

5. Conclusions

The microstructure of plain CAC was studied under controlled time–temperature histories in order to describe and quantify different phase assemblages of hydrates in presence or not of Li_2SO_4.

- The hydration kinetics of CAC seems to be controlled by space availability. This hypothesis experimentally based on isothermal calorimetry and chemical shrinkage [28] requires further investigation in progress and based on microstructural modelling using the platform model *μic* [29].
- The hydration of cement paste with controlled self heating gives interesting and new results on the microstructural development. First, the degree of CA hydration after 24 h between isothermal 38 °C and self heating to 50 °C is comparable (around 85%) but the growth of C_2AH_8 plates and AH_3 differs and leads to higher microporosity in case of self heating. Secondly, the study of C_3AH_6 and AH_3 assemblage at 70 °C showed that space filling is mainly controlled by the crystal structure and density of AH_3 polymorph. The progressive self heating to 70 °C rather promotes the precipitation of low density AH_3 and subsequent lower porosity while the straight curing at 70 °C leads to precipitation of denser AH_3.
- The hydration of secondary siliceous reactants such as C_2AS showed that the pore volume change induced during the dissolution of metastable C_2AH_8 plates can be controlled by the simultaneous precipitation of C_2ASH_8 from C_2AS hydration. The hydration of C_2AS seems to be controlled by the space available subsequently to the early age formation of products. C_2ASH_8 was mainly observed in the cement grains (intermixed with C_3AH_6) but also in the pore space replacing C_2AH_8 plates. It was generally observed that C_3AH_6 precipitates first in the cement grains replacing CA sites, and only at later ages at the edge of C_2AH_8 plates.
- The main effect of Li_2SO_4 addition concerns the homogeneous nucleation of hydrates throughout the solution space. The even distribution of C_2AH_8 plates was clearly observed in isothermal 38 °C hydration in presence of very small amounts of Li_2SO_4 (0.012%$_{wt}$). In contrast the nucleation of C_2AH_8 is longer, leading to a separate heat generation peak, and the distribution of hydrates remains uneven throughout the microstructure. The nucleation effect of Li_2SO_4 is generally attributed to the formation of intermediate lithium aluminate hydrate but this phase was not identified in this condition of dosage. In contrast, it was clearly shown that Li_2SO_4 promotes the precipitation of the more stable and denser hydrates regardless of the phase assemblage obtained after 24 h. Nonetheless this result seems to be partly contradictory with the quantification approach on the degree of CA hydration which showed that Li_2SO_4 addition lowers the hydration of CA at temperatures of hydration ranging 20 to 50 °C.

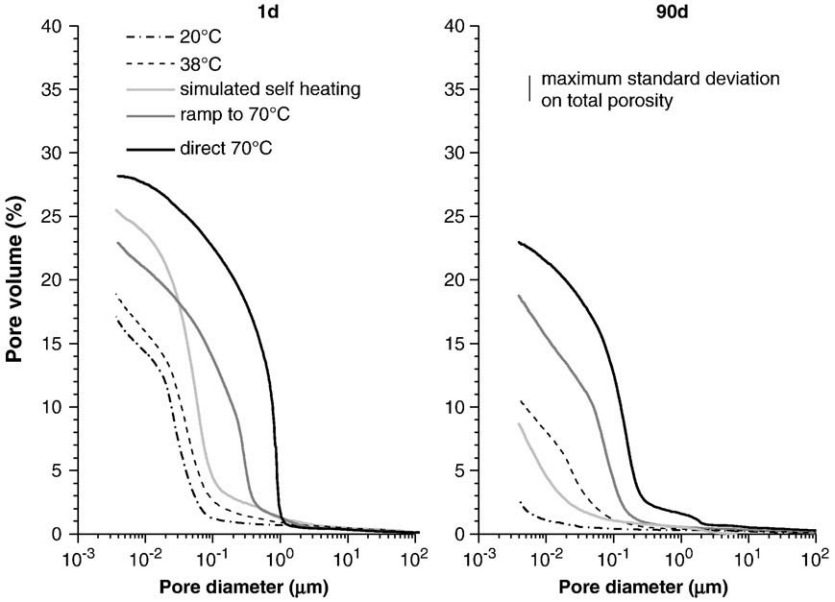

Fig. 16. Total porosity *vs* pore diameter from MIP of CAC paste with 0.012%$_{wt}$ Li_2SO_4 after 1 d hydration with different time–temperature histories and after 90 d curing under water at 20 °C.

Acknowledgements

The authors gratefully acknowledge Kerneos Company (France) for the financial support of this project and the supply of raw materials.

References

[1] K.L. Scrivener, A. Capmas, Calcium aluminate cements, Chapter 13, in: P.C. Hewlett (Ed.), Lea's Chemistry of Cement and Concrete, John Wiley & Sons, New York, 1998.
[2] H. Pöllmann, Mineralogy and crystal chemistry of calcium aluminate cement, Calcium Aluminates Cements, Proceedings of the International Symposium, Edinburgh, Scotland, UK, 2001, pp. 79–119.
[3] K.L. Scrivener, H.F.W. Taylor, Microstructural development in pastes of a calcium aluminate cement, Calcium Aluminate Cement, Chapman and Hall, London, 1990, pp. 41–51.
[4] A.J. Majumdar, B. Singh, R.N. Edmonds, Hydration of mixtures of $C_{12}A_7$ and granulated blastfurnace slag, Cement and Concrete Research 19 (6) (1989) 848–856.
[5] B. Singh, A.J. Majumdar, K. Quillin, Properties of BRECEM ten-year results, Cement and Concrete Research 29 (3) (1999) 429–433.
[6] J. Ding, Y. Fu, J.J. Beaudoin, Stratlingite formation in high alumina cement–silica fume systems: significance of sodium ions, Cement and Concrete Research 25 (6) (1995) 1311–1319.
[7] S. Bentsen, A. Seltveit, B. Sanderg, Effect of microsilica conversion of high alumina cement, Calcium Aluminates Cements, Proceedings of the International Symposium, London, UK, 1990, pp. 294–334.
[8] H.G. Midgley, P. Bhaskara Rao, Formation of stratlingite, $2CaO.SiO_2.Al_2O_3.8H_2O$, in relation to the hydration of high alumina cement, Cement and Concrete Research 8 (2) (1978) 169–172.
[9] D. Damidot, A. Rettel, D. Sorrentino, A. Capmas, Action of admixtures on Fondu cement: II. Effect of lithium salts on the anomalous setting time observed for temperatures ranging from 18 to 35 °C, Advances in Cement Research 9 (35) (1997) 127–134.
[10] F. Goetz-Neunhoeffer, Hydration kinetics of calcium aluminate cement in presence of Li_2CO_3, Calcium Aluminate Cements The Centenary Conference, BRE Press, Avignon, France, 2008, pp. 181–196.
[11] S.A. Rodger, D.D. Double, The chemistry of hydration of high alumina cement in the presence of accelerating and retarding admixtures, Cement and Concrete Research 14 (1) (1984) 73–82.
[12] E. Sadok, Rôles comparés des cations étrangers en solution dans l'étape de germination associée à l'hydratation des sulfates de calcium et de l'aluminate monocalcique, PhD, 1989, Institut National des Sciences Appliquées de Lyon.
[13] D. Damidot, A. Rettel, A. Capmas, Action of admixtures on Fondu cement: Part 1. Lithium and sodium salts compared, Advances in Cement Research 8 (31) (1996) 111–119.
[14] P. Barret, D. Bertrandie, Minimum instability curve in metastable solution of CA, 7th International Conference on Cement Chemistry, Editions Septima, Paris, 1980, p. 134.
[15] C. Gosselin, K.L. Scrivener, Microstructure development of calcium aluminate cement accelerated with lithium sulphate, Calcium Aluminate Cements The Centenary Conference, BRE Press, Avignon, France, 2008, pp. 109–122.
[16] M.T. Gaztañaga, S. Goñi, A. Guerrero, Accelerated carbonation of calcium aluminate cement paste, Calcium Aluminates Cements, Proceedings of the International Symposium, 2001, pp. 349–359, Edinburgh, Scotland, UK.
[17] A. Hidalgo, S. Petit, J.L. García, C. Alonso, C. Andrade, Microstructure of the system calcium aluminate cement–silica fume: application in waste immobilization, Studies in Surface Science and Catalysis (2007) 1617–1628.
[18] H. Fryda, F. Saucier, S. Lamberet, K. Scrivener, D. Guinot, La durabilité des bétons d'aluminates de calcium, Chapter 14, La durabilité des bétons, ENPC, 2008, pp. 767–823.
[19] F. Moro, H. Böhni, Ink–bottle effect in mercury intrusion porosimetry of cement-based materials, Journal of Colloid and Interface Science 246 (1) (2002) 135–149.
[20] C. Galle, Effect of drying on cement-based materials pore structure as identified by mercury intrusion porosimetry. A comparative study between oven-, vacuum-, and freeze-drying, Cement and Concrete Research 31 (10) (2001) 1467–1477.
[21] S. Diamond, Mercury porosimetry: an inappropriate method for the measurement of pore size distributions in cement-based materials, Cement and Concrete Research 30 (10) (2000) 1517–1525.
[22] R.A. Olson, C.M. Neubauer, H.M. Jennings, Damage to the pore structure of hardened Portland cement paste by mercury intrusion, Journal of the American Ceramic Society 80 (9) (1997) 2454–2458.
[23] A. Capmas, D. Ménétrier-Sorrentino, D. Damidot, Effect of temperature on setting time of calcium aluminate cements, Calcium Aluminate Cements, Chapman and Hall, London, 1989, pp. 65–80.
[24] P. Barret, D. Ménétrier, D. Bertrandie, Contribution to the study of the kinetic mechanism of aluminous cement setting I — latent periods in heterogeneous and homogeneous milieus and the absence of heterogeneous nucleation, Cement and Concrete Research 4 (4) (1974) 545–556.
[25] P. Barret, D. Ménétrier, Contribution to the study of the kinetic mechanism of aluminous cement setting II — release of the factor responsible for breaking the latent period by the dissolution of a fraction of the initial cement, Cement and Concrete Research 4 (5) (1974) 723–733.
[26] K. Fujii, W. Kondo, H. Ueno, Kinetics of hydration of monocalcium aluminate, Journal of the American Ceramic Society 69 (4) (1986) 361–364.
[27] T.G. Jappy, F.P. Glasser, Synthesis and stability of silica-substituted hydrogarnet $Ca_3Al_2Si_{3-x}O_{12-4x}(OH)_{4x}$, Advances in Cement Research 4 (1) (1991/92) 1–8.
[28] J. Ideker, Early-age behaviour of calcium aluminate cement systems, PhD, 2008, University of Austin, Texas.
[29] S. Bishnoi, K.L. Scrivener, μic: a new platform for modelling the hydration of cements, Cement and Concrete Research 39 (4) (2009) 266–274.
[30] G. Renaudin, Etude d'un hydroxyde simple d'aluminium: La bayerite, II. Etude d'une famille d'hydroxydes doubles lamellaires d'aluminium et de calcium: Les phases AFm (aluminate tetracalciques hydratés), PhD, 1998, University Henri Poincaré.
[31] J.M. Tait, A. Violante, P. Violante, Co-crystallization of gibbsite and bayerite with Nordstrandite, Clay Minerals 18 (1983) 95–99.